An Approximate Thermal Analysis of Stirling Engine Regenerators

S.H. Park* and Y.-S. Lee**

(Received October 24, 1992)

This paper approximates the transport phenomena in a Stirling engine regenerator to aid its practical design. The mass flow rates are simplified by a square-wave function and the pressure variations, by a saw-tooth function with a phase difference. Approximate analytical solutions obtained in this study agree well with the available numerical solutions. Using the approximate solutions of the transport phenomena the entropy generation rates in a regenerator are analytically formulated and calculated, which come from axial conduction loss, imperfect heat regeneration, and pressure drop due to fluid friction. The geometry of the minimum entropy generation rate can represent the optimal design parameters of the regenerator.

Key Words: Stirling Engine Regenerator, Entropy Generation, Axial Conduction Loss, Imperfect Heat Regeneration, Pressure Drop

Nomenclature

a : Heat transfer area per unit volume
A_a, A_b : Defined in appendix
B_a, B_b : Defined in appendix
C : Inertia coefficient
C_a, C_b : Defined in appendix
C_P : Gas specific heat at constant pressure
C_S : Solid specific heat
C_t : Coefficient for h_t
C_V : Gas specific heat at constant volume
C_{1a}, C_{1b} : Defined in Eq. (13)
d : Wire diameter
d_h : Mesh hydraulic diameter
D : Regenerator diameter
D_a, D_b : Defined in appendix
e : Internal energy
E_a, E_b : Defined in appendix
G : Dimensionless mass flux
$\dot{G}$: Mass flux
G_m : Mean value of mass flux
h : Enthalpy
h_t : Heat transfer coefficient
k : Thermal conductivity
K : Permeability
K_h : Proportionality factor for h_t
L : Regenerator length
M : Working gas mole number
n : Exponent for h_t
P : Pressure
P_o : Defined in Eq. (41)
$\bar{P}$: Dimensionless pressure
$\dot{q}$: Conduction heat flux
R : Gas constant
Re_h : Hydraulic Reynolds number
Re_P : Reynolds number defined in Eq. (41)
$\Delta S''$: Entropy generation per unit area per cycle
$\Delta \dot{S}_{Mole}$: Molar entropy generation rate
t : Time
T : Temperature
U : Gas velocity
w : Dimensionless axial distance
x : Axial distance
ε : Matrix porosity
ϕ : Shape factor
γ : Specific heat ratio
η : Effectiveness
μ : Viscosity
θ : Dimensionless temperature

* Department of Mechanical Engineering, Hong-Ik University, Seoul, 121-791, Korea
** Waste Heat Utilization Research Team, Korea Institute of Energy Research, Taejon, Korea

ρ : Density
τ : Time span of a full cycle
τ_1 : Time phase angle between pressure and mass flux

Superscripts

$\cdot$: per unit time
$''$: per unit area

Subscripts

0 : at $x=0$
a : for intervals I and III
b : for intervals II and IV
C : Conductive
e : Effective
f : Working gas
h : Hydraulic
H : Maximum in P
L : at $x=L$ or minimum in P
P : Hydraulic friction
s : Solid matrix
T : Heat exchange

1. Introduction

A Stirling cycle engine is a mechanical device that operates on a regenerative thermodynamic cycle, with cyclic compression and expansion of the working fluid at different temperature levels. It covers machines capable of operating a prime mover, heat pump, refrigerating engine, etc. (Walker, 1980). A regenerator interconnecting the high and low temperature parts in the system is used to increase the system thermal efficiency, receiving the energy from the working gas flowing from the high temperature part to the low temperature part and returning the stored energy to the working gas returning from the low temperture part to the high temperture part. In addition, its periodic operation makes the system relatively insensitive to plugging by condensible impurities(Ackermann and Gifford, 1969; Sahoo and Sarangi, 1988).

The role of the regenerator is simple and its structure is compact. It, however, is a large amount of work to analyze the internal transport phenomena exactly and to utilize the analysis in designing the regenerator, since the temperature, pressure, and flow vary significantly during the operation. The object of this study is, therefore, to simplify the phenomena, to obtain their analytical solutions based on the first-law analysis and the entropy generation rates based on the second-law analysis, and to find the optimal geometric conditions under which the entropy generation rate is minimum.

These cyclically varying phenomena were analyzed by Rea and Smith(1967) with the simplification of stepwise mass flux and saw-tooth pressure variations in phase. Qvale and Smith(1968) derived an approximate closed-form solution for the thermal performance of a Stirling-engine regenerator for sinusoidal mass flow rate and pressure variations with a phase difference relative to mass flux, using the temperature distribution assumed by a quadratic polynomial. Modest and Tien (1973, 1974) considered the effects of real gas behavior, solid matrix conduction, and finite matrix heat capacity, showing that the gas-conduction effects are negligible but the solid-matrix conduction can be significant. Using the finite element method, Datta(1985) conducted a dynamic analysis of a Stirling engine regenerator with a phase angle 90°. Gedeon(1985) took a first step to develop a mathematical model for multidimensional gas flow in the system. Harris et al.(1970) discussed the design method of a regenerator through the decoupling of the irreversibilities based on the first law of thermodynamics. Chen et al.(1984) applied the linear harmonic analysis to obtain a semi-closed-form solution to the governing equations and used the second-law analysis to provide a rational method for allocating overall efficiency losses to different loss mechanisms. Kuo(1989) numerically calculated the transport phenomena including the thermal dispersion effect of the working gas and also suggested the optimal designing method based on the second law of thermadynamics. Since numerical approaches are more or less involved, a simple analytical results are often demanded in a practical design. Therefore, the object of this research is to obtain simple analytical results of the phenomena and to do an analysis based on the second

law of thermodynamics.

In the present paper the mass flow rates are simplified by a square-wave function and the pressure variations, by a saw-tooth function with a phase difference to mass flux. While the governing equations are simplified based on the previous work done by Rea and Smith(1967), the solutions are approximated algebraically and compared with the numerical solutions which were in good agreement with the experimental measurements (Rea and Smith, 1967). Using the approximate solutions of the transport phenomena the entropy generation rates in a regenerator are analytically obtained, which are due to axial conduction loss, imperfect heat regeneration, and pressure drop due to fluid friction. The geometrical conditions such as aspect ratio, porosity, mesh size, etc., giving the minimum entropy generation rate can represent the optimal design parameters of the regenerator with respect to irreversibilities. In addition, the entropy generation rates of three common working gases : hydrogen, helium, and air under the same working condition are calculated to compare their physical characteristics.

2. First-Law Analysis

2.1 Governing equations

Figure 1(a) shows the schematic diagram for a regenerator of diameter D, length L, and end temperatures T_0 and T_L, which is packed with porosity ε by woven screens of stainless-steel-wire diameter d. In Fig. 1(b) the mass flux at $x=0$, $\dot{G}_0$, of the working gas varies stepwise and the system pressure P does in a saw-tooth shape with a time difference τ_1, in which the period is τ.

The governing equations of the transport phenomena in a regenerator can be derived by considering the conservations of mass, momentum, and energy over a differential control volume.

Gas Continuity

$$\frac{\partial \dot{G}}{\partial x}=-\frac{1}{R}\frac{\partial}{\partial t}\left(\frac{P}{T_f}\right), \tag{1}$$

Gas Momentum

$$\frac{\partial P}{\partial x}=-\frac{\mu\varepsilon}{K}U_f-C\rho_f\varepsilon^2U_f^2, \tag{2}$$

Gas Energy

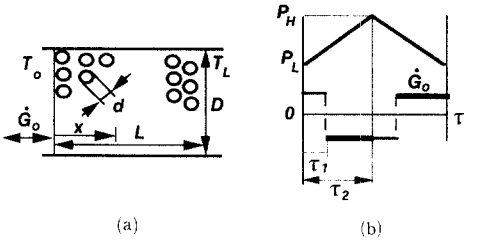

Fig. 1 (a) Schematic of a regenerator
(b) Cyclic variations of pressure and mass flux at $x=0$ with a time-phase difference τ_1

$$\frac{C_v}{R}\frac{\partial P}{\partial t}+C_p\frac{\partial}{\partial x}(\dot{G}T_f)=\frac{h_t a}{\varepsilon}(T_s-T_f), \tag{3}$$

Gas State

$$P=\rho_f RT_f, \tag{4}$$

Solid Matrix Energy

$$\rho_s C_s\frac{\partial T_s}{\partial t}=\frac{h_t a}{1-\varepsilon}(T_f-T_s), \tag{5}$$

where the permeability and inertia coefficient can be written (Tanaka and Chisaka, 1988) as

$$K=\frac{32\varepsilon^3d^2}{175\ \phi^2(1-\varepsilon)^2}\ \text{and}\ C=\frac{1.6\phi(1-\varepsilon)}{8\varepsilon^3d}, \tag{6}$$

Here, the shape factor ϕ is 4 for columns(wire netting), 6.9 for triangular prism(sponge metal), and 6 for spheres. The heat transfer coefficient h_t and specific surface area a can be expressed, respectively, as

$$h_t=\frac{C_t k_f Re_h^n Pr^{\frac{1}{3}}}{d_h}\ \text{and}\ a=\frac{4\varepsilon}{d_h}, \tag{7}$$

where d_h is the hydraulic diameter of the matrix, given as $d_h=\dfrac{4\varepsilon d}{\phi(1-\varepsilon)}$ In this study, the constant C_t and the exponent n are 0.33 and 0.67, respectively, although they can vary (Ergun, 1952 ; Rea and Smith, 1967).

Boundary conditions for Eqs. (1),(3) and (5) are

$$\text{at } x=0\begin{cases}\dot{G}=\dot{G}_o(t),\\ T_s=T_o,\\ T_f=T_o\ (0\le t\le\tau_1\ \text{and}\ (\tau_1+\tau_2)\le t\le\tau),\end{cases}$$
$$\text{at } x=L\begin{cases}T_s=T_L,\\ T_f=T_L\ (\tau_1\le t\le\tau_1+\tau_2).\end{cases} \tag{8}$$

2.2 Assumptions and modeling

The assumptions made in Eqs. (1)~(5) are

(1) The process is one-dimensional and thus, the

radial heat conduction loss to the wall is negligible.

(2) The working gas behaves like a perfect gas.

(3) Axial conduction heat transfer is negligible in the first law analysis.

(4) Thermophysical properties of the working gas and solid matrix are constant.

(5) Since $\int_0^L \frac{\partial P}{\partial x} dx \ll \int_0^{\tau/2} \frac{\partial P}{\partial t} dt$, the pressure drop in the regenerator is neglected in the first law analysis and thus the terms on the right hand side of Eq. (2) disappear.

(6) Since $\frac{|T_f - T_s|}{T_s} \ll 1$, $\frac{\partial (P/T_f)}{\partial t} \cong \frac{dP/dt}{T_s}$

(7) The directions of the flow inside the regenerator vary simultaneously with those of the flow at $x=0$.

Under the cyclic-steady operation, the following conditions are maintained at any position x.

$$\oint \dot{G} dt = 0, \tag{9}$$

$$\oint \frac{\partial P}{\partial t} dt = 0, \tag{10}$$

$$\oint \rho_s C_s \frac{\partial T_s}{\partial t} dt = \oint \frac{h_t a}{1-\varepsilon} (T_f - T_s) dt = 0, \tag{11}$$

$$\oint G T_f dt = const. \tag{12}$$

The cyclic integral $\oint$ can be subdivided into four time-interval integrals such as $\int_0^{\tau 1}$ (period I) $+\int_{\tau 1}^{\tau/2}$ (II) $+\int_{\tau/2}^{\tau/2+\tau 1}$ (III) $+\int_{\tau/2+\tau 1}^{\tau}$ (IV). Based on the assumption (7) Eqs.(11) and (12) are approximated as

$$\begin{aligned} &T_{fI} + T_{fIII} = 2T_{sa}, \\ &T_{fII} + T_{fIV} = 2T_{sb}, \\ &\dot{G}(T_{fIII} - T_{fI}) = C_{1a}, \\ &\dot{G}(T_{fII} - T_{fIV}) = C_{1b}, \end{aligned} \tag{13}$$

where the subscripts a and b represent the pairs of intervals I and III and intervals II and IV, respectively.

For intervals (I) and (III), the governing equations become

$$C_p \frac{d}{dx}(\dot{G} T_{fI}) - \frac{h_t a}{\varepsilon}(T_s - T_{fI}) + \frac{C_v}{R}\left|\frac{dP}{dt}\right| = 0, \tag{14}$$

$$-C_p \frac{d}{dx}(\dot{G} T_{fIII}) - \frac{h_t a}{\varepsilon}(T_s - T_{fIII}) - \frac{C_v}{R}\left|\frac{dP}{dt}\right| = 0, \tag{15}$$

$$\frac{d\dot{G}}{dx} = -\frac{1}{RT_s}\left|\frac{dP}{dt}\right|, \tag{16}$$

and are simplified by subtracting Eq. (15) from Eq. (14) and with Eqs. (13) and (16) as

$$\dot{G}\frac{dT_{sa}}{dx} - \frac{h_t a C_{1a}}{2\varepsilon C_p \dot{G}} - \frac{1}{C_p}\left|\frac{dP}{dt}\right| = 0, \tag{17}$$

$$\frac{d\dot{G}}{dx} = -\frac{1}{RT_{sa}}\left|\frac{dP}{dt}\right|. \tag{18}$$

For intervals (II) and (IV), the governing equations are simplified through the same procedure as above and the resulting equations are

$$\dot{G}\frac{dT_{sb}}{dx} - \frac{h_t a C_{1b}}{2\varepsilon C_p \dot{G}} + \frac{1}{C_p}\left|\frac{dP}{dt}\right| = 0, \tag{19}$$

$$\frac{d\dot{G}}{dx} = \frac{1}{RT_{sb}}\left|\frac{dP}{dt}\right|. \tag{20}$$

To solve the simplified equations the three boundary conditions (8) are required because C_{1a} or C_{1b} is still unknown and must be determined from a boundary condition.

2.3 Nondimensionalization and approximate solutions

To solve Eqs. (17)~(20) the following nondimensional variables are introduced

$$\theta = \frac{T_s}{T_o}, \quad G = \frac{\dot{G}}{\dot{G}_o}, \quad w = \frac{\left|\frac{dP}{dt}\right| x}{\dot{G}_o R T_o}. \tag{21}$$

Also, the convection heat transfer coefficient is correlated as $h_t = K_h G^n$ where $K_h = 0.33\, k_f\, Re_{h0}^n\, Pr^{\frac{1}{3}}/d_h$ Now, the governing equations become for intervals (I and III)

$$G\frac{d\theta}{dw} = C_{oa} G^{n-1} + \frac{\gamma - 1}{\gamma}, \tag{22}$$

$$\theta\frac{dG}{dw} = -1, \tag{23}$$

for intervals(II and IV)

$$G\frac{d\theta}{dw} = C_{ob} G^{n-1} - \frac{\gamma - 1}{\gamma}, \tag{24}$$

$$\theta\frac{dG}{dw} = 1, \tag{25}$$

where $C_{oa} = \frac{(\gamma-1) K_h a C_{1a}}{2\gamma\varepsilon \dot{G}_o \left|\frac{dP}{dt}\right|}$ and

$$C_{ob} = \frac{(\gamma-1) K_h a C_{1b}}{2\gamma\varepsilon \dot{G}_o \left|\frac{dP}{dt}\right|}.$$

Boundary conditions become

at $w=0: G=1, \theta=1,$

at $w=w_{max}=\dfrac{\left|\dfrac{dP}{dt}\right|L}{G_o R T_o}: \theta=\dfrac{T_L}{T_o}=\theta_L.$ (26)

Assuming that pressure and mass flux variations are in phase, Rea and smith(1967) obtained Eqs. (24) and (25). They solved numerically and showed the results graphically for various C_{ob}. However, the numerical solutions are difficult to use furthermore. In this study, therefore, analytical solutions for temperature and mass flux are obtained approximately for the easy application of the analysis to the practical design of the regenerators.

In Eqs. (22) and (24), G^{n-1} is approximated by its mean value G_m^{n-1}, where G_m is assumed as $[1+G(w_{max})]/2$ for intervals (I) and (III) and as $2/[1+1/G(w_{max})]$ for intervals (II) and (IV), which result in a favorable approximation to the numerical solutions. Then, addition of Eqs. (22) to (23) and integration of the resulting equation give

$$G=(C_{4a}w+1)^{-\frac{1}{C4a}}, \quad (27)$$

$$\theta=A_a(C_{4a}w+1)^{B_a}+C_a(C_{4a}w+1)^{D_a}+E_a, \quad (28)$$

for intervals (I) and (III) and following the same procedure as above gives

$$G=(C_{4b}w+1)^{-\frac{1}{C4b}}, \quad (29)$$

$$\theta=A_b(C_{4b}w+1)^{B_b}+C_b(C_{4b}w+1)^{D_b}+E_b, \quad (30)$$

for intervals (II) and (IV), where $C_{4a}=C_{oa}G_m^{n-1}$

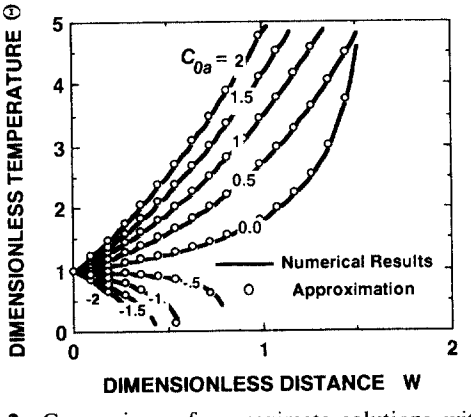

Fig. 2 Comparison of approximate solutions with numerical simulation results for the temperature distribution in the intervals I and III

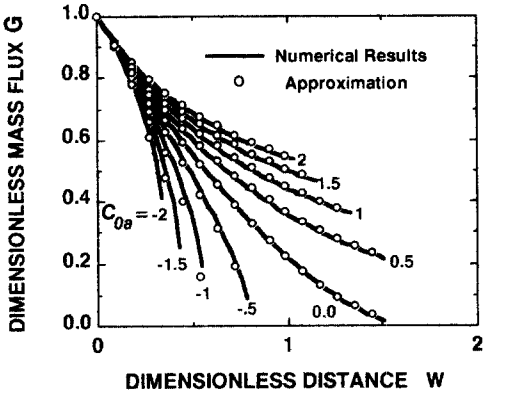

Fig. 3 Comparison of approximate solutions with numerical simulation results for the mass flux distribution in the intervals I and III

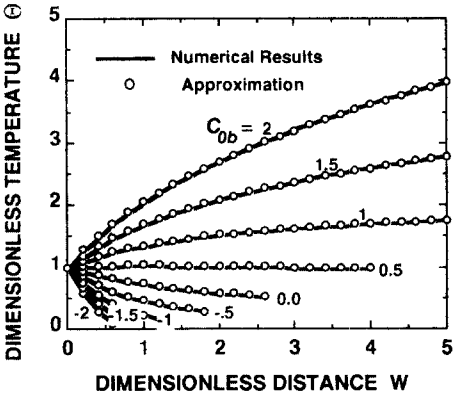

Fig. 4 Comparison of approximate solutions with numerical simulation results for the temperature distribution in the intervals II and IV

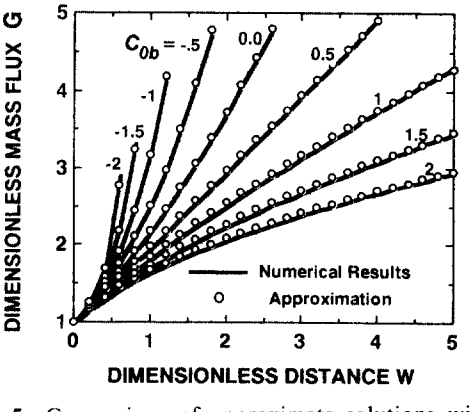

Fig. 5 Comparison of approximate solutions with numerical simulation results for the mass flux distribution in the intervals II and IV

$-1/\gamma$ and $C_{4b}=C_{ob}G_m^{n-1}+1/\gamma$ and other constants are shown in the appendix. The constants C_{oa} and C_{ob} can be obtained by the boundary condition $\theta_L=\theta(w_{max})$. They, however, cannot be explicitly expressed and thus, are shown graphically in Figs. 2 and 4. In Figs. 2~5 the approximate analytic solutions are compared with the numerical solutions, which are solved by the Runge-Kutta method and are in good agreement with the experimental results (Rea and Smith, 1967), and result in errors less than three percents. Therefore, the approximate solutions will be used to formulate and to calculate the regenerator effectiveness and the entropy generation rates through the second-law thermodynamic analysis.

2.4 Regenerator effectiveness.

The ineffectiveness of thermal regenerator is defined as (Kays and London, 1964; Modest and Tien, 1973)

$$1-\eta=\frac{\text{cyclic total losses}}{\text{cyclic ideal heat exchange}}, \tag{31}$$

where η is the thermal effectiveness. Equation (31) can be written mathematically as

$$1-\eta=\frac{\varepsilon\oint\dot{G}h\ dt+\oint k_e\frac{\partial T_s}{\partial x}dt}{\varepsilon\left[\oint_{I,\ IV}|\dot{G}|h\ dt|_{x=0}-\int_{II,\ III}|\dot{G}|h\ dt|_{x=L}-\int_0^L\rho_f e\ dx\Big|_{t=\tau1+\tau2}^{t=\tau1}\right]}, \tag{32}$$

where intervals (I) and (IV) are the hot gas flow ones and intervals (II) and (III) are the cold gas flow ones. The numerator of Eq. (32) is constant over the entire length of the regenerator (Modest and Tien, 1973), if the conduction term is considered in the energy equations. The last term in the denominator describes the difference of internal energy of the gas in the regenerator at the ends of hot gas and cold gas blow intervals. Using the appoximate solutions Eq. (32) can be simplified as

$$1-\eta=\frac{\varepsilon(-\tau_1C_pC_{1a}-\tau_2C_pC_{1b})+2\tau_1\dot{q}_{oa}+2\tau_2\dot{q}_{ob}}{\varepsilon\left[\tau_1C_p(\dot{G}_0T_0-\dot{G}_{La}T_L)+\tau_2C_p(\dot{G}_0T_0-\dot{G}_{Lb}T_L)-\frac{L}{\gamma-1}(P_{\tau1}-P_{\tau1+\tau2})\right]}, \tag{33}$$

where effective conductivety is $k_e=k_f(k_s/k_f)^{(1-\varepsilon)0.59}$ (Chang, 1990). Here, conduction heat fluxes at $x=0$ are

$$\dot{q}_{0a}=-C_q\left(C_{0a}+\frac{\gamma-1}{\gamma}\right), \tag{34}$$

$$\dot{q}_{0b}=-C_q\left(C_{0b}-\frac{\gamma-1}{\gamma}\right), \tag{35}$$

where $C_q=\frac{k_e\left|\frac{dP}{dt}\right|}{\dot{G}_0R}$. Figure 6 shows the effectiveness with regenerator lengths for the Ford 4-215 Stirling engine (Urielli and Berchowitz, 1984). Smaller the mesh size is, higher the effectiveness is, since the heat transfer area a between the fluid and the solid matrix is reciprocally proprotional to the mesh size d.

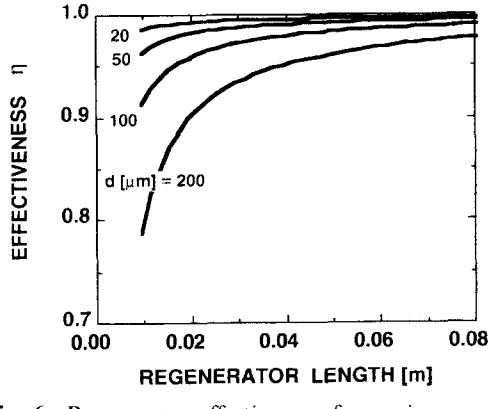

Fig. 6 Regenerator effectiveness for various mesh sizes

3. Second-Law Analysis

3.1 Entropy generation.

Because the ineffectiveness defined by Eq. (33) fails to consider the hydraulic friction loss and thus, it does not indicate a certain optimal geometric conditions, it is an insufficient measure of regenerator performance. A second-law analysis can supply a better measure from which a Stirling

engine design can minimize any source of irreversibility or entropy generation. Entropy generation per cycle per unit area in the regenerator (Bejan, 1982) can be calculated from

$$\Delta S''=\left[\oint\varepsilon\dot{G}C_p ln(T)dt-\oint\varepsilon\dot{G}Rln(P)dt+\oint\frac{\dot{q}}{T}dt\right]_{x=L}-\left[\oint\varepsilon\dot{G}C_p ln(T)dt-\oint\varepsilon\dot{G}Rln(P)dt+\oint\frac{\dot{q}}{T}dt\right]_{x=0}, \quad (36)$$

where $\dot{q}$ is the conduction heat flux which consists of both the gas conduction and soild matrix conduction.

3.2 Simplification.

Equation (36) can be simplified as follows. The terms including $ln(T)$ are reduced to

$$\oint\dot{G}C_p ln(T)dt\cong-\frac{\tau_1 C_p C_{1a}}{T}-\frac{\tau_2 C_p C_{1b}}{T}, \quad (37)$$

with the approximation $ln(1+\delta)\cong\delta$ for $\delta\ll 1$. Thus, entropy generation due to imperfect heat exchange is

$$\Delta S_T''=\varepsilon C_p(C_{1a}\tau_1+C_{1b}\tau_2)(\frac{1}{T_0}-\frac{1}{T_L}). \quad (38)$$

Entropy generation due to conduction heat transfer at $x=0$ and L is approximated as

$$\Delta S_c''=2[\frac{\dot{q}_{La}\tau_1+\dot{q}_{La}\tau_2}{T_L}-\frac{\dot{q}_{0a}\tau_1+\dot{q}_{0b}\tau_2}{T_0}]. \quad (39)$$

Pressure drop across the bed, which was neglected in the first law analysis but must be considered in the second law analysis, can be obtained from the momentum Eq. (2) using the non-Darcian model. Through nondimensionalization, it becomes

$$\frac{d\bar{P}^2}{dw}=-G\theta-Re_p G^2\theta, \quad (40)$$

where

$$\bar{P}=\frac{P}{P_o},\quad P_o=\dot{G}_0 RT_0\sqrt{\frac{2\mu\varepsilon}{K|\frac{dP}{dt}|}},$$

and $$Re_p=\frac{C\varepsilon\dot{G}_0 K}{\mu}. \quad (41)$$

By integrating Eq. (40) and with the approximation $\bar{P}_L^2-\bar{P}_0^2\cong 2\bar{P}\Delta\bar{P}$

for intervals (I) and (III) $\Delta\overline{P_a}=-\frac{\Delta\overline{P_a'}}{2\bar{P}}$,

for intervals (II) and (IV) $\Delta\overline{P_b}=-\frac{\Delta\overline{P_b'}}{2\bar{P}}$, (42)

where

$$\Delta\overline{P_a'}=(C_{4a}\frac{w_{max}^2}{2}+w_{max})+\frac{Re_p}{2C_{4a}-1}(C_{4a}w_{max}+1)^{(2-\frac{1}{C_{4a}})}-\frac{Re_p}{2C_{4a}-1}, \quad (43)$$

and

$$\Delta\overline{P_b'}=(C_{4b}\frac{w_{max}^2}{2}+w_{max})+\frac{Re_p}{2C_{4b}-1}(C_{4b}w_{max}+1)^{(2+\frac{1}{C_{4b}})}-\frac{Re_p}{2C_{4b}+1}. \quad (44)$$

Entropy generation due to hydraulic friction can be approximated as

$$\Delta S_p''=-\varepsilon[\int_{II+III}\dot{G}R\frac{\Delta\bar{P}}{\bar{P}}dt\,|_{x=0}+\int_{I+IV}\dot{G}R\frac{\Delta\bar{P}}{\bar{P}}dt|_{x=L}], \quad (45)$$

and thus

$$\Delta S_p''=\frac{\varepsilon G_0 R}{2}[\Delta\bar{P}_a'(G_a(w_{max})\int_0^{\tau 1}\frac{1}{\bar{P}^2}dt+G_0\int_{\tau 2-\tau 1}^{\tau 2}\frac{1}{\bar{P}^2}dt)+\Delta\bar{P}_b'(G_0\int_{\tau 1}^{\tau 2}\frac{1}{\bar{P}^2}dt+G_b(w_{max})\int_0^{\tau 2-\tau 1}\frac{1}{\bar{P}^2}dt)], \quad (46)$$

where

$$\int_{\tau i}^{\tau j}\frac{1}{\bar{P}^2}dt=\frac{\tau}{2(\bar{P}_H-\bar{P}_L)}[\frac{1}{\bar{P}_L+\frac{2\tau_i(\bar{P}_H-\bar{P}_L)}{\tau}}-\frac{1}{\bar{P}_L+\frac{2\tau_j(\bar{P}_H-\bar{P}_L)}{\tau}}]. \quad (47)$$

Therefore, the molar entropy generation rate in the regenerator is

$$\Delta\dot{S}_{Mole}=\frac{\pi D^2\Delta S''}{4\tau M}, \quad (48)$$

where M is the mole number of the working fluid entering at $x=0$ and $\Delta S''=\Delta S_T''+\Delta S_C''+\Delta S_P''$.

3.3 Results and discussion.

The physical model in calculating entropy generation rates comes from the Ford 4-215 engine whose working gas is hydrogen (Urieli and Berchowitz, 1984). Its geometric conditions and physical variables used in this study are shown in Table 1. Solid matrix properties are based on stainless steel and gas properties are on the algebraic mean temperature of high and low temperature parts.

Table 1 Parameters used in the calculation of regenerator effectiveness and entropy generation rates.

d	36	mm	P_H	20	MPa
D	73	mm	T	1023	K
Frequency		4000 rpm	T_L	337	K
L	34	mm	working gas		H_2
M	0.2	mole	ε	0.62	
P_L	11	MPa	τ_1	$\tau/2$	

Figures 7 (a)~(c) show the entropy generation rates $\Delta\dot{S}_{Mole}$, $\Delta\dot{S}_T$, $\Delta\dot{S}_c$, and $\Delta\dot{S}_p$ with regenerator lengths for the time-phase difference $\tau_1=0$, $\tau/4$, and $\tau/2$. Irreversibility due to hydraulic friction, $\Delta\dot{S}_p$, increases with lengths as expected in Eq. (42). Its slope for $\tau_1=\tau/2$ in Fig. 7(c) is not as steep as that for $\tau_1=0$ in Fig. 7(a), because the gas is compressed during the hot gas blowing and is expanded during the cold gas blowing and thus, the mass flux reduces along the regenerator for the case of $\tau_1=\tau/2$. Irreversibility due to imperfect heat exchange, $\Delta\dot{S}_T$, decreases, since $C_{0a,b}$ and $C_{1a,b}$ decrease with lengths. That due to conduction heat transfer at both ends of the regenerator, $\Delta\dot{S}_c$, decreases monotonously for $\tau_1=0$ in Fig. 7(a). For $\tau_1=\tau/2$ in Fig. 7(c), however, it decreases once and increase significantly, since the conduction loss at $x=L$, $\dot{q}_{La}$, in Eq. (39) increases significantly for negative C_{0a} with lengths as indicated in Fig. 2, while the loss at $x=0$, $\dot{q}_{0a}$, decreases. For interval (I) under the subscript 'a' the system pressure increases during the hot gas blowing. Thus, the gas inside the regenerator is compressed, less amount of gas exits the regenerator, and the inside temperature becomes higher. To satisfy the temperature boundary condition at $x=L$ the slope there becomes steeper, though it becomes less steep if heat conduction terms were included in energy equations. The effect of inertia drag expressed by C in Eq. (2) can be emphasized by comparing the solid line and the symbolic line in Fig. 7(b). The total entropy generation rate $\Delta\dot{S}_{Mole}$ locates its minimum near 0.04 m which tells the optimal length of the regenerator. Although the differ-

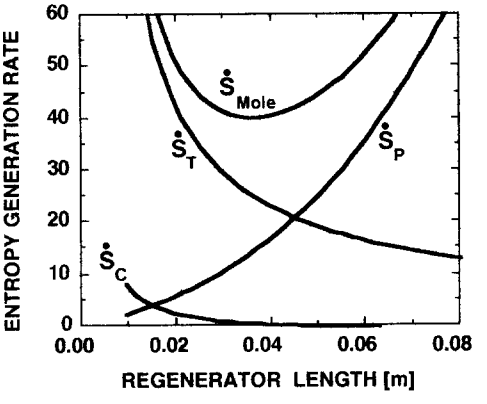

(a)

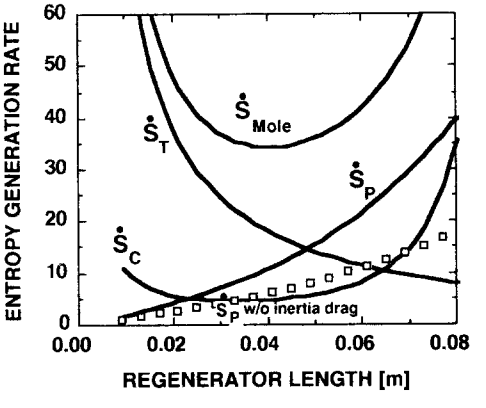

(b)

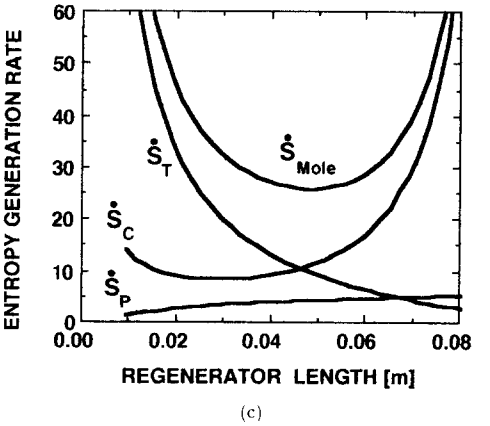

(c)

Fig. 7 (a) Entropy generation rates with lengths for $\tau_1=0$
(b) Entropy generation rates with lengths for $\tau_1=\tau/4$
(c) Entropy generation rates with lengths for $\tau_1=\tau/2$

ences of $\Delta\dot{S}_{Mole}$ between $\tau_1=0$ and $\tau/2$ are not negligible, the influence of the phase difference cannot be related to the regenerator design directly, since the phase difference is determined mainly by the total mechanism of the Stirling engine, not by the regenerator itself.

The variation of $\Delta\dot{S}_{Mole}$ with aspect ratio L/D for the dead volume of the Ford 4-215 engine is indicated in Fig. 8 for various mesh sizes and in Fig. 9 for three working gases. In Fig. 8 $\Delta\dot{S}_{Mole}$ decreases once and increases for small d, and it decreases slower for large d and is expected to increase for large values of L/D. Here, the velocity increase with L/D and thus, the irreversibility due to heat transfer decreases with L/D which describes the early decrease of $\Delta\dot{S}_{Mole}$, while that from pressure drop increases which results in the later increase of $\Delta\dot{S}_{Mole}$.

Figures 9~11 show $\Delta\dot{S}_{Mole}$ for three kinds of gases commonly used in the Stirling system : air, hydrogen, and helium. For smaller heat exchange area between the working gas and the solid matrix, helium is the best due to its high conductivity ; on the other hand, for larger contact area hydrogen is the best due to its lower viscosity. However, the differences of minimum irreversibilities between helium and hydrogen are not great as shown in the figures. In addition, they also indicate that the change of entropy generation near the minimum is small compared to the

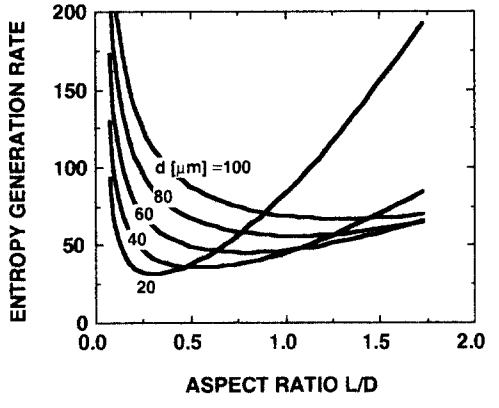

Fig. 8 Entropy generation rates with aspect ratios for various mesh sizes

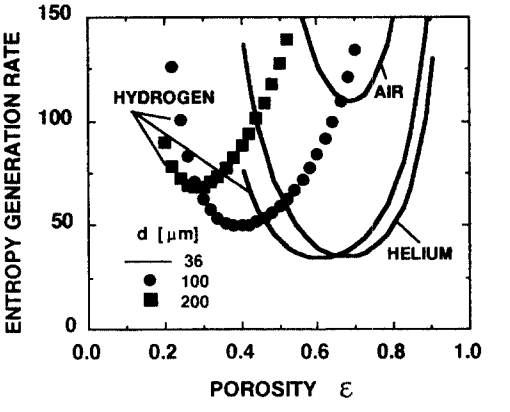

Fig. 10 Entropy generation rates with porosities for different mesh sizes and gases

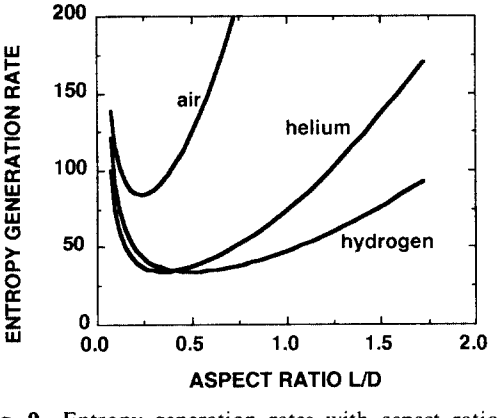

Fig. 9 Entropy generation rates with aspect ratios for different gases

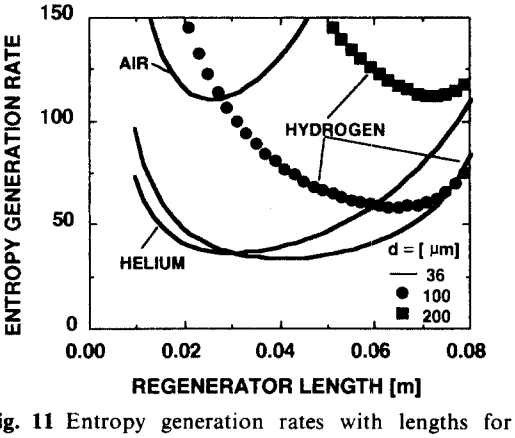

Fig. 11 Entropy generation rates with lengths for different mesh sizes and gases

span of independent variables. Therefore, we can have large flexibility in designing the regenerator. In Figs. 8, 10~11 symbolic lines depict $\Delta\dot{S}_{Mole}$ for larger mesh sizes than that of the Ford engine. It can be noticed that even for larger mesh sizes we can have low $\Delta\dot{S}_{Mole}$ comparable to those for smaller sizes, though the optimal conditions move to increase the heat exchange area considerably.

4. Conclusion

Appoximate analytic solutions are obtained which are in good agreement with the numerical solutions for a saw-tooth-type pressure variation and a square-wave-type mass flow variation with a phase. The resulting solutions are used to analytically express the regenerator ineffectiveness and entropy generation rates.

The second law analysis identifies three sources of irreversibility such as the imperfect heat exchange, heat conduction loss at both ends, and hydraulic friction which is described by the non-Darcian momentum equation. The resulting entropy generation charts are extremely useful for the optimal design of a regenerator. Finally, future study is recommended on the effect of lateral heat transfer to the regenerator housing.

References

Ackermann, R.A. and Gifford, W.E., 1969, "Small Cryogenic Regenerator Performance," ASME Journal of Engineering for Industry, pp. 273~281.

Bejan, A., 1982, Entropy Generation through Heat and Fluid Flow, John Wiley & Sons, New York.

Chang, W.S., 1990, "Porosity and Effective Thermal Conductivity of Wire Screens," ASME Journal of Heat Transfer, Vol. 112, pp. 5~9.

Chen, N.C.J., Griffin, F.P. and West, C.D., 1984, "Linear Harmonic Analysis for Stirling Machines and Second Law Analysis of Four Important Losses," Proceedings of the 19th ICECE, Paper No. 849141, pp. 2015~2020.

Datta, S., 1985, "Computational Techniques in Finite Element Analysis of a Stirling Engine Regenerator," Proceedings of the 20th ICECE, Paper No. 859433, pp. 3349~3353.

Ergun, S., 1952, "Fluid Flow through Packed Columns," Chemical Engineering Progress, Vol. 48, pp. 89~94.

Gedeon, D., 1985, "Computational Techniques for the Two-Dimensional Gasdynamic Equations in Stirling Engine Regenerators and Associated Manifolds," Proceedings of the 20th ICECE, Paper No. 859434, pp. 3354~3359.

Harris, W.S., Rios, P.A. and Smith, J.L., Jr., 1970, "The Design of Thermal Regenerators for Stirling-Type Refrigerators," Advances in Cryogenic Engineering, Vol. 16, pp. 312~323.

Kays, W.M. and London, A.L., 1964, Compact Heat Exchangers, McGraw-Hill, New York, N.Y.

Kuo, S.M., 1989, "Convective Heat Transfer through Complex Structures," Ph.D. Dissertation, University of California, Berkeley.

Modest, M.F. and Tien, C.L., 1973, "Analysis of Real-Gas and Matrix-Conduction Effects in Cyclic Cryogenic Refrigerators," ASME Journal of Heat Transfer, Vol. 95, pp. 199~205.

Modest, M.F. and Tien, C.L., 1974, "Thermal Analysis of Cyclic Cryogenic Refrigerators," International Journal of Heat and Mass Transfer, Vol. 17, pp. 37~49.

Qvale, E.B. and Smith, J.L. Jr. 1968, "A Mathematical Model for Steady Operation of Stirling-Type Engines," ASME Journal of Engineering for Power, Vol. 90, pp. 45~50.

Rea, S.N. and Smith, J.L. Jr., 1967, "The Influence of Pressure Cycling on Thermal Regenerators," ASME Journal of Engineering for Industry, Vol. 89, pp. 563~569.

Sahoo, R.K. and Sarangi, S., 1988, "The Effect of Condensible Impurities in the Working Fluid on the Performance of Cryogenic Regenerators," ASME Journal of Heat Transfer, Vol. 110, pp. 77~83.

Tanaka, M. and Chisaka, F., 1988, "Thermal Performance of Regenerator," Proceedings of the 4th ICSE, pp. 375~380.

Urieli, I., and Berchowitz, D.M., 1984, Stirling Cycle Engine Analysis, Adam Hilger, Bristol.

Walker, G., 1980, Stirling Engines, Clarendon Press, Oxford.

Appendix

The constants for the approximate solutions in Eqs. (27)~(30) are

$$A_a=\frac{C_{0a}}{C_{4a}-(n-2)},$$

$$B_a=1-\frac{n-2}{C_{4a}},$$

$$C_a=\frac{\gamma-1}{\gamma}\frac{1}{C_{4a}+1},$$

$$D_a=1+\frac{1}{C_{4a}}$$

$$E_a=1-A_a-C_a,$$

$$A_b=\frac{C_{0b}}{C_{4b}+(n-2)},$$

$$B_b=1+\frac{n-2}{C_{4b}},$$

$$C_b=-\frac{\gamma-1}{\gamma}\frac{1}{C_{4b}-1},$$

$$D_b=1-\frac{1}{C_{4b}},$$

$$E_b=1-A_b-C_b.$$